



The Role of Redox Hopping in Metal-Organic Framework Electrocatalysis

Journal:	<i>ChemComm</i>
Manuscript ID	CC-FEA-02-2018-001664.R1
Article Type:	Feature Article

SCHOLARONE™
Manuscripts



Journal Name

FEATURE ARTICLE

The Role of Redox Hopping in Metal-Organic Framework Electrocatalysis

Received 00th January 20xx,
Accepted 00th January 20xx

Shaoyang Lin,^a Pavel M. Usov,^a and Amanda J. Morris^{* a}

DOI: 10.1039/x0xx00000x

www.rsc.org/

The dominant charge transfer mechanism in a vast number of metal organic frameworks (MOFs) is that of redox hopping, a process best explained through the motion of electrons via self-exchange reactions between redox centres coupled to the motion of counterbalancing ions. Mechanistic studies of redox hopping transport in MOFs reveal characteristics that recall pioneering studies in linear redox polymers. When MOFs are employed as electrocatalysts, consideration must be given to both the catalytic properties – turnover frequency (TOF) and energetic requirements (overpotential, TON) – and the charge transport properties – rate of charge hopping, measured via an apparent diffusion coefficient (D_{app}). Herein, we provide a mathematical framework to provide constraints to MOF catalyst development by relating D_{app} , TOF, and film thickness in the context of providing 10 mA/cm² of catalytic current. Lastly with the mechanistic studies discussed as a foundation, design rules for future MOF electrocatalysts are provided and the challenges to the community to optimize MOF charge transport are laid out.

endeavor due to its contribution to the exploration of future commercially viable artificial photosynthesis systems. In the context of global energy issues, the search for alternative energy sources to replace currently utilized fossil fuels is one of the most pressing challenges of our generation. Efficient solar energy conversion/storage using water splitting and CO₂ reduction, mimicking nature's photosynthetic process, is a promising pathway to address this pressing energy problem. One of the key obstacles towards the development of efficient catalysts is overcoming the slow kinetics and high thermodynamic barrier for these electrochemical transformations. Incorporating these catalytic systems into MOF scaffolds could afford novel electrocatalytic materials with increased stability, reusability and turnover frequency (TOF) per unit of electroactive area compared to its homogeneous counterpart. The development of these materials could pave the way for the future realization of photoelectrochemical solar energy conversion devices. Currently, MOF-based electrocatalysts have been reported for several different reactions, including water oxidation,²¹⁻²⁸ oxygen reduction,²⁹⁻³¹ hydrogen reduction,³²⁻³⁴ and CO₂ reduction.³⁵⁻³⁹

1. Introduction

Metal-organic frameworks (MOFs) have been extensively investigated in recent years because of their many unique properties, such as large surface area, ordered crystalline structure, high chemical and structural stabilities, and synthetic tunability, among others. In particular, recent developments in manipulating electronic and electrochemical properties of MOFs have led to several candidate materials for a variety of applications, historically outside the scope of mainstream MOF research.¹ These include, but are not limited to, thermoelectronics,²⁻⁴ photovoltaics,⁵⁻⁸ semiconductors,⁹⁻¹¹ capacitors,¹²⁻¹⁵ and electrochemical catalysis.¹⁶⁻²⁰

The development of MOF electrocatalysts has been an important

Despite the great potential for MOFs to impact electrocatalytic applications, the intrinsically low conductivity of the great majority of reported MOFs remains the major limitation for the efficient charge transport necessary to support catalysis.³⁹ Several moderately conductive frameworks were reported exhibiting outstanding performance in terms of TOF and chemical stability. Compared to the homogeneous catalyst (over the same time period), a 26-fold increase of catalytic turnover number (TON) was observed for a cobalt porphyrin containing framework utilized for electrochemical CO₂ reduction.³⁷ A MOF thin film stable in alkaline conditions, MAF-X27-OH reported by Chen et al. for electrochemical water oxidation supplied catalytic current as high as 10 mA/cm² for more than 24 h.²⁴ What is particularly interesting, however, is the fact that the conductivities of these MOFs are only 1×10^{-6} S cm⁻¹ and 2.2×10^{-9} S cm⁻¹, respectively. This means that through-framework electronic delocalization is likely insufficient to supply the necessary charge. In the first example, the charge transport properties were indicative of a diffusion controlled redox hopping process. This Cottrell-like behavior was also observed for other MOF thin film

^a Department of Chemistry and Macromolecules Innovation Institute, Virginia Polytechnic Institute and State University, Blacksburg, Virginia 24061, United States

* ajmorrison@vt.edu

materials. Therefore, it is proposed that redox-hopping alone could facilitate an efficient charge propagation from the electrode to the active catalytic centers within the framework structures.

To assess this hypothesis, herein, we will first discuss the charge transport pathways in MOFs. Then the research about redox hopping in polymer thin films will be summarized, as shown in previous studies related to MOFs, with charge hopping as the main charge transport pathway. In addition, the importance of redox hopping in the context of MOF electrocatalysts will be examined. Finally, the interplay between the redox hopping rate and electrocatalytic reaction rate in MOF-based systems is discussed by evaluating the minimum apparent charge diffusion coefficient, D_{app} , required to supply the benchmark catalytic current density of 10 mA/cm^2 , which is sufficient for a future solar fuel device to reach 10% energy conversion efficiency.^{40,41}

2. Charge Transport in MOFs

Facile charge migration is required for efficient MOF electrocatalysts; otherwise, the reaction would only occur at the catalytic centers in direct proximity to the electrode. The rate of electron movement is determined by the nature of the charge transport pathway. Besides super-exchange^{42,43} and tunneling,⁴⁴ charge transport in MOFs can be generally rationalized in terms of the following two mechanisms: band transport or charge hopping.⁴⁵⁻⁴⁷ As summarized earlier, a high degree of electronic delocalization between the framework components is required for the band mechanism to be operative, whereas localized charge carriers (such as redox centers) often result in the charge hopping process.^{45,46} Increasing the extent of delocalization by introducing donor-acceptor type interactions⁴⁸⁻⁵¹, mixed valent states of the node/linker,^{52,53} π - π stacking or π -conjugation into the framework could lead to improved charge propagation. In general, three main strategies have been employed in the design and synthesis of MOF with enhanced charge transport properties.

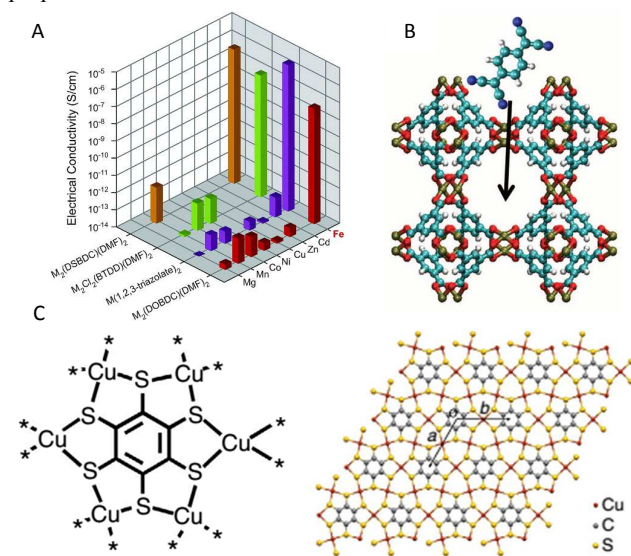


Figure 1. (A) Comparison of electrical conductivities of select MOFs, demonstrating that Fe analogues generally exhibit higher

values. (M – metal node, H_4DOBDC = 2,5-dihydroxybenzene-1,4-dicarboxylic acid, H_4DSBDC = 2,5-disulfhydrylbenzene-1,4-dicarboxylic acid, BTDD = bis(1H-1,2,3-triazolo[4,5-b],[4',5'-i]dibenzo[1,4]dioxin));⁵⁴ (B) Incorporation of TCNQ into the pore of $[\text{Cu}_3(\text{BTC})_2]$ MOF giving rise to a highly conductive framework-guest composite;⁵⁵ (C) Structure of the 2D Cu-BHT framework.⁵⁶

(1) Guest-host interaction

Incorporation of guest-host interaction via post-synthetic modifications of existing MOFs can increase the charge mobility.⁵⁷⁻⁶⁰ Long et al. utilized I_2 vapor as a chemical oxidant to achieve a mixed valence state in $\text{Cu}[\text{Ni}(\text{pdt})_2]$ (pdt^{2-} = pyrazine-2,3-dithiolate) MOF, resulting in a 10^4 fold increase in conductivity.⁶¹ The relatively high conductivity of this material was aided by a high degree of electronic delocalization across the $[\text{Ni}(\text{pdt})_2]^{2-}$ building units. Incorporation of redox-active guests could also lead to the formation of new charge transport pathways throughout the extended structure. In 2014, Talin and Allendorf et al. demonstrated that infiltration of TCNQ (7,7,8,8-tetracyanoquinodimethane) into a Cu-based MOF, HKUST-1 (Figure 1B) causes a dramatic increase in conductivity from 10^{-8} to 0.07 S cm^{-1} .⁵⁵ It was postulated that binding of TCNQ to Cu_2 paddlewheel nodes, coupled with partial charge transfer between the framework and the guests, resulted in the formation of charge conduits extending throughout the structure. Moreover, guest incorporation could be used to directly modulate the charge transport properties in MOFs. Given that β -CD (β -cyclodextrin) shows great affinity to ferrocene but low affinity to ferrocenium, Hupp et al. reported that the apparent charge diffusion coefficient of a ferrocene-infiltrated NU-1000 framework measured during the electrochemical cycling was tuned by up to 30 times through the introduction of guest molecules at different concentration.⁵⁹

(2) Judicious choice of the metal node and linker

A key consideration in the design process is the orbital overlap between the framework components.⁶²⁻⁶⁴ As such, atoms and ions with diffuse frontier orbitals, such as softer transition metal ions (Fe, Mn, Co, Ni and Cu) and ligand atoms (N and S), are particularly suitable for the construction of highly delocalized MOFs. For example, charge transport was found to occur through an infinite 1D (-Mn-O-) chain in $\text{Mn}_2(\text{DOBDC})$ (H_4DOBDC = 2,5-dihydroxybenzene-1,4-dicarboxylic acid). By replacing the oxygen atom with a sulfur atom, and forming an infinite 1D (-Mn-S-) chain in the framework, energy mismatch was decreased and charge delocalization enhanced. The resultant MOF material $\text{Mn}_2(\text{DSBDC})$ (H_4DSBDC = 2,5-disulfhydrylbenzene-1,4-dicarboxylic acid) exhibited higher charge mobility than its original analog.⁶³ In another example, Dincă et al. reported that mixed valence $\text{Fe}^{\text{II/III}}$ nodes improved the charge density throughout the framework. The corresponding MOFs exhibited at least 5 orders higher conductivity compared to the analogous structures (Figure 1A) comprised of different metal centers (Mg, Mn, Co, Ni, Cu, Zn and Cd).^{54,63,65}

(3) π - π interactions

Π - π interactions introduce through-space electronic delocalization, providing an additional conduction pathway. In this scenario, spatial positioning and orientation of framework components become

increasingly important. Extended π -stacks and π -conjugation can be highly efficient at charge transport. This type of conduction mechanism was first reported in molecular charge transfer complexes, such as TTF-TCNQ, which were the first examples of purely organic materials exhibiting metallic conductivity.⁶⁶ A similar structural motif has been incorporated into MOFs with functionalized TTF (tetrathiafulvalene) derivatives receiving particular attention.⁶⁷⁻⁶⁹ The π - π stacking of TTF moieties resulted in the formation of highly conductive charge transport columns. By adjusting the size of metal ions in the coordination environment, S-S distance between the TTF units could be modified to increase the orbital overlap, leading to improved conductivity.⁶⁹ Another type of π - π interaction, in-plane π -conjugation, introduces charge delocalization in the 2D MOF.⁷⁰⁻⁷⁵ The 2D MOF Cu-BHT (BHT = benzenehexathiol), reported by Zhu et al. in 2015, displays great charge delocalization due to extended 2D π -conjugation, which exhibits conductivity as high as 1580 S cm⁻¹ at room temperature (Figure 1C).^{46, 56}

Utilizing the aforementioned strategies, the design of conductive frameworks was recently reviewed.⁴⁵⁻⁴⁷ Overall, it is clear that the π - π strategy has resulted in the largest increase in conductivity.

3. Redox Hopping in Linear Redox Polymers Revisited

While a few MOFs have been specifically designed for enhanced charge transport capabilities, there are numerous reported frameworks exhibiting moderate conductivity based on charge hopping. For MOF based electrocatalysts, the overall charge transport processes involve not only the flow of electrons throughout the framework, but also the kinetics of the catalytic cycle, the transport of the reactants and products, and the diffusion of counter-ions.^{46, 76} These processes are paralleled in polymer thin films coated on electrodes, which were previously studied for their redox hopping behavior.^{77, 78} In a similar fashion to MOFs, the redox centers in linear redox polymers are distributed throughout the polymer matrix as discrete sites.

Electroactive species, for example [Ru(bpy)₃]²⁺,⁷⁹ TTF⁸⁰ or ferrocene⁸¹ were incorporated into polymer thin films via *in situ* or post-synthetic methods. Different fabrication methods, including electropolymerization and spin casting were employed for deposition of polymers as thin films on electrode surfaces.⁸²⁻⁸⁴ The charge transport behavior of these films was typically characterized using electrochemical and spectroscopic techniques,⁸⁵ among others.⁸⁶ In the late 1970s, Murray and Kaufman et al. first proposed that the primary charge transfer mechanism in these polymers is redox hopping between the neighboring redox centers. Since then, there have been numerous reports that try to understand the nature of the hopping process, which is briefly summarized as follows.^{80, 84, 87, 88}

Charge transport across the polymer thin film can be defined in terms of a diffusion process obeying Fick's law. Redox reactions in polymers occur via electron hopping or electron self-exchange between electroactive sites, coupled with counter-ion diffusion inside the films to maintain electroneutrality. The overall charge transport rate can be described by an apparent diffusion coefficient,

D_{app} , which was first proposed by Dahms and Ruff et al.⁸⁹⁻⁹¹ (D-R equation) and further interpreted and modified by Anson,⁸³ Bard,⁷⁹ Saveant et al.^{92, 93} (Equations 1a and 1b):

$$D_{app} = D_0 + D_{ex} \quad (1a)$$

$$D_{ex} = kC\delta^2/6 \quad (1b)$$

where D_0 is the diffusion coefficient contributed by the physical displacement of electroactive species and counter-ions. D_{ex} is the self-exchange/electron hopping rate, k is the dinuclear self-exchange constant, C is the concentration of the active sites, and δ is the site to site distance. Measurement of the physical diffusion coefficient of the redox centers and the D_{app} revealed that the charge transport is likely limited by ion/molecule diffusion or self-exchange electron transfer (charge hopping).^{79, 88, 94} Follow-up studies revealed that, as the loading level of electroactive sites in the polymer matrix increases to a certain threshold level, the D_{app} exhibits a rapid increase.^{81, 93, 95} It was found that D-R equation could not fully explain the concentration dependent variation of D_{app} . In later reports, the description of charge propagation was improved by taking the effects of ion association and percolation theory into account.^{93, 96-99} The in-depth details of the theoretical studies involving these processes will not be discussed beyond this point. From here on, we would like to focus on the results that are relevant to the redox hopping process in MOFs.

(1) Critical role of counter-ions

During the cyclic voltammetry (CV) experiments, slow ion diffusion into the polymer matrix is responsible for the non-ideal shape of the observed CV wave.^{84, 100} An activation step or a break-in process (Figure 2A), in which the current continuously increased with each cycle until reaching a steady state, was also attributed to slow counter-ion diffusion and electron hopping rate compared to the voltammogram timescale.⁸⁴ Moreover, electrolyte properties play an important role in governing the electrochemical response of polymer thin films. Additional factors, such as ion pairing⁸¹, mobility, and the concentration of counter-ions^{86, 101} can cause pronounced effects on the voltammetric response and charge transport rate.

(2) Solvent swelling effect

Unlike MOFs, however, thin films based on polymers do not exhibit permanent porosity, yet they allow for the counter-ion permeation to occur.^{84, 86} When the solvent swells the polymer matrix, not only is the formation ion diffusion channels observed,^{81, 87} but also the distance between electroactive sites¹⁰² increases. Therefore, this process could have an opposing effect on the resultant current response, either increasing or decreasing it. Due to the relatively high rigidity of MOF structures compared to polymers, it is reasonable to assume that the solvent swelling effect would be negligible. However, MOF crystal engineering could lead to an effect equivalent to solvent swelling by tuning the pore size and the distance between redox sites.

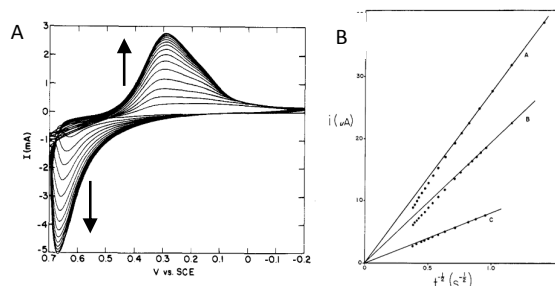


Figure 2. (A) Cyclic voltammograms of TTF loaded polymer film measured in 0.1 M TEAP/CH₃CN (TEAP = Tetraethylammonium perchlorate) with a scan rate of 100 mV/s, demonstrating the “break in” process.⁸⁶ (B) Cottrell plots of polymer thin films coated onto electrode with different loading of [Ru(bpy)₃]²⁺.¹⁰⁰

(3) Scan rate dependent CV analysis

Dependency between peak current (I_p) and peak separation (ΔE_p) in CV and scan rate (v) could be used as a diagnostic criteria for distinguishing surface confined vs. diffusion controlled redox reactions.^{87, 103} When the peak current is primarily generated from a diffusion control redox hopping, it should obey the Randles–Sevcik equation (Equation 3):

$$I_p = 0.4463nFAC(nFvD/RT)^{1/2} \quad (3)$$

On the other hand, if I_p is originated from surface bound redox species, it should follow Equation 4,

$$I_p = n^2F^2vA\Gamma/4RT \quad (4)$$

where n is the number of electrons transferred, F is the Faraday constant, A is the electrode surface area, C is the concentration of the redox-active species in the polymer thin film, D is the diffusion coefficient, R is the molar gas constant, T is the absolute temperature and Γ is the amount of active species adsorbed on the electrode. Interestingly, these two scenarios are not mutually exclusive, and the same material could exhibit either of the scan-rate dependence behaviors at different scan rates. Bard et al. reported that a 100 nm Nafion film containing 2.2 nmol/cm² [Ru(bpy)₃]²⁺ exhibited a surface confined behavior at slower scan rates (< 30 mV/s). However, at higher scan rates the voltammetric response of the material switched to bulk diffusion characteristic (Figure 2B).¹⁰⁰

(4) Semi-infinite vs finite diffusion

Chronoamperometry is a highly convenient method for elucidating D_{app} . Semi-infinite-diffusion-based Cottrell behavior was observed in most studied cases.¹⁰³ D_{app} can be calculated from the slope of i_p versus $t^{1/2}$ plot. It is important to note that the linear region in this graph is usually only valid at the early stages of a potential step.^{100, 103} The relationship deviates from a linear trend with increasing

reaction time, as the thickness of the diffusion layer approaches the thickness of the polymer thin film.¹⁰⁰ This behavior suggests a transition from semi-infinite diffusion model (linear region) to finite diffusion (non-linear region).^{81, 104}

4. Redox Hopping Behavior in MOFs

It was discovered that the electrochemical behavior in a vast number of MOFs displays great similarity with that of redox polymer films. Valuable insights and guidelines for interrogating the redox hopping behavior in MOFs to be used in electrochemical applications could be obtained from the aforementioned studies. The recent studies on the redox hopping process of MOFs are summarized and ordered in a similar fashion to the polymer section.

The nature of electrolyte plays an important role in governing electrochemical behavior of MOFs. Furukawa et al. reported that changing the electrolyte from (n-Bu₄N)BF₄ to (n-Bu₄N)NO₃ resulted in a negative shift of the redox potential of ferrocene/ferrocenium couple (from 0.95 to 0.78 V vs Ag/AgCl) incorporated inside the MOF, {[Zn(Fcdc)(bpy)](DMF)_{0.5}(MeOH)_{0.5}]_n (Fcdc = 1,1'-ferrocenedicarboxylate).¹⁰⁵ The authors assigned this potential shift to the stronger ion pairing effect between NO₃⁻ and ferrocenium, lowering the ferrocene oxidation potential. In a closely related study, Farha and Hupp et al. reported a bias-switchable ion permselectivity in ferrocene installed NU-1000 (Fe-NU-1000) MOF thin films. At low electrolyte concentration (0.05 M (n-Bu₄N)PF₆), the electrogenerated ferrocenium cations inside the MOF will block the infiltration of cation ion (Figure 3A).¹⁰⁶ Since the onset oxidation potential for the linker of NU-1000, TBzPy (1,3,6,8-tetrakis(p-benzoate)pyrene, 1.5 V vs Ag/AgCl) is higher than that for ferrocene (0.8 V vs Ag/AgCl), positive counter-ions were unable to diffuse to the linker due to the exclusion effect cause by the oxidized ferrocene. When the concentration of (n-Bu₄N)PF₆ (0.5 M) in solution is higher than ferrocenium in the framework (0.3 M), the charge of the overall structure returned to neutral, allowing the cations to infiltrate. As a result, the oxidation of the TBzPy linker could occur at the expected oxidation potential.

The break-in process was also observed in the CV of electrochemically active MOF thin film. Dinca et al. employed a solvothermal deposition method to fabricate [Zn(NDI-X)] (NDI = naphthalene diimide, X = H, SEt, NHET) framework as thin films on FTO electrodes for applications in electrochromic windows.¹⁰⁷ This method generally results in more robust films, compared to mechanical immobilization of MOF particles. Evidence for diffusion limited charge transport can be observed in the multi-cycle CV experiment, where a steady increase in the peak current for reduction of [Zn(NDI-H)] can be observed over the course of 50 cycles until reaching a plateau (Figure 3B). Compared to an unfunctionalized NDI core, the SEt analogue exhibited a constricted pore space, resulting in less favorable counter-ion diffusion. Thus, it required more time (longer scan cycle) to access all the electroactive sites within the framework, similar to the break-in process observed in polymer thin films.

The redox hopping pathways in MOFs were studied via scan rate dependent CV analysis. In 2011, Marken et al. reported a study on

redox processes of the ferrocenyl groups in post synthetically modified MOF, $[\text{Zn}_4\text{O}(\text{bpdc-NH}_2)_3]$ ($\text{H}_2\text{bpdc-NH}_2 = 2\text{-aminobiphenyl-4,4'-dicarboxylic acid}$).¹⁰⁸ The sample was attached to the basal plane pyrolytic graphite electrode by rubbing the electrode surface with the MOF powder. Variable scan-rate CV experiments were carried out in 0.1 M (n-Bu₄N)PF₆/dichloroethane electrolyte. The position and separation of the ferrocene reduction and oxidation peaks was found to be independent of the scan rate. Moreover, the dependency of peak current (i_p) and scan rate (v) was found to be $i_p \propto v^{0.78}$. These results led the author to conclude that the redox process was facilitated by the charge hopping confined to the MOF particle surface. In another example, D'Alessandro et al. found that the charge hopping could operate throughout the entire framework. In their study, redox active MOF powder $[\text{Zn}_2(\text{NDC})_2(\text{DPNI})]$ ($\text{NDC} = 2,7\text{-naphthalene dicarboxylate}$, $\text{DPNI} = \text{N,N'-di(4-pyridyl)-1,4,5,8-naphthalenetetracarboxyldiimide}$) was deposited onto an ITO-coated quartz electrode (ITO = indium tin oxide) using mechanical immobilization for electrochemical and spectroelectrochemical studies.¹⁰⁹ Under a reducing potential bias, the color change of the MOF, detected by diffuse reflectance UV-Vis-NIR spectroscopy, provided further evidence for in-MOF diffusion controlled redox reaction.

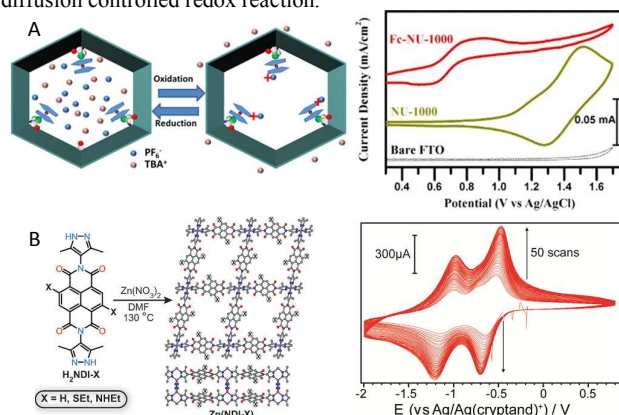
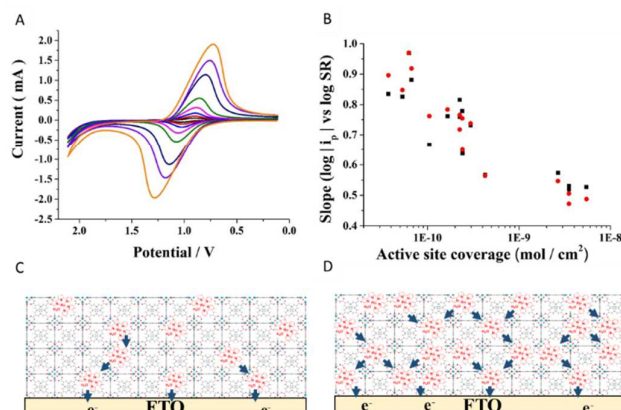


Figure 3. (A) Scheme of cationic exclusion effect in oxidized ferrocene doped NU-1000 and CV of the corresponding thin film.¹⁰⁶ (B) Structure of $[\text{Zn}(\text{NDI-SEt})]$ and the CV data of the MOF film on FTO electrode measured in 0.1 M (n-Bu₄N)PF₆/DMF electrolyte using 100 mV/s scan rate, showing overlapping voltammograms.¹⁰⁷

The MOF composition was also used to modify the transition between surface-confined and bulk redox hopping. Morris and co-workers reported a $[\text{Ru}(\text{tpy})(\text{dcbpy})\text{OH}_2]^{2+}$ modified UiO-67 (Ru-UiO-67, tpy = 2,2':6',2''-terpyridine, dcbpy = 5,5'-dicarboxy-2,2'-bipyridine) thin film grown on an FTO electrode using a solvothermal method, and employed the film for electrochemical water oxidation.²³ During the synthesis of Ru-UiO-67, the ratio of the catalyst $[\text{Ru}(\text{tpy})(\text{dcbpy})\text{OH}_2]^{2+}$ and the backbone linker BPDC (biphenyl-4,4'-dicarboxylic acid) was varied to modulate the catalyst loading.^{23, 110} To evaluate the amount of electroactive sites, a potential step was applied to the Ru-UiO-67 thin films to oxidize the Ru centers from +2 to +4 oxidation state. The charge passed during this process was recorded. The number of electroactive Ru complexes within the films was estimated from the total charge passed during the potential step. The values ranged from 3.8×10^{11}

to 1.2×10^{18} mol cm⁻² across the films with different loadings. In order to further elucidate these results, a scan rate dependent voltammetry study was conducted on Ru-UiO-67 thin films with different active site coverage. The plot of $\log(i_p)$ vs $\log(\text{scan rate})$ provides a clue to the nature of the redox process and charge propagation. The slope of this plot was found to decrease from 1 to 0.5 as the active site coverage level increased (Figure 4A, 4B). It was postulated that, at a low active site coverage level, site-to-site charge hopping was limited by long average distances between the



Ru centers. Thus, the current response was mostly due to the oxidation of Ru catalysts in direct proximity to the electrode surface. As the electroactive species concentration increased, more pathways for charge hopping became available. Therefore, the current contribution from redox hopping gradually increased until it became the dominant component of the electrochemical response (Figure 4C).

Figure 4. (A) Cyclic voltammograms of Ru-UiO-67 thin film measured at scan rates ranging from 10 to 1000 mV/s; (B) The slope of the $\log |i_p|$ (red, cathodic peak; black, anodic peak) against $\log(\text{scan rate})$ with respect to active site coverage; proposed charge transport pathways in Ru-UiO-67 thin films with low (C) and high (D) electroactive site coverage.²³

These results highlighted the importance of further mechanistic studies of the diffusion limited redox hopping phenomena that directly influence the electrochemical and electrocatalytic properties in MOFs. In previous reports, metalloporphyrins were identified as ideal moieties for spectroelectrochemistry characterization due to their distinctly varied spectra in different oxidation states. By conducting solid state spectroelectrochemistry analysis, Morris et al. reported the first systematic study of the redox hopping mechanism of a MOF thin film (CoPIZA). This thin film was solvothermally grown on FTO substrates, which contains CoTCPP (5,10,15,20-(4-carboxyphenyl)porphyrin)Co^{III}, Figure 5A).¹¹¹ CV experiments were performed on the resultant films using 0.1 M LiClO₄/DMF as a supporting electrolyte. Two cathodic peaks were detected at -1.1 V and -1.45 V vs ferrocyanide and assigned to the consecutive reductions of the metal centers inside the porphyrin core, Co^{III/II}TCPP, and Co^{II/I}TCPP, respectively. The first cathodic peak was accompanied by an anodic peak at -0.975 V and was ascribed to the reversible wave for Co^{III/II}TCPP redox couple. The peak current i_{pc} at -1.1 V, recorded at different scan rates, was linear to $v^{1/2}$ and

not *v.* As discussed before, the square root dependence indicates a diffusion limited redox hopping process. The absorption spectra of CoPIZA at different applied potentials were recorded. By fitting the difference of absorption values (ΔA) at 419 nm for the $\text{Co}^{\text{II/I}}\text{TCPP}$ (CoPIZA) redox couple to a modified Cottrell equation (Equation 5, Figure 5B), the apparent diffusion constant D_{app} was calculated to be $7.55(\pm 0.05) \times 10^{-14} \text{ cm}^2/\text{s}$.

$$\Delta A = 2A_{\text{max}}D_{\text{app}}^{1/2}t^{1/2}/d\tau^{1/2} \quad (5)$$

A similar charge hopping behavior was demonstrated in a related cobalt porphyrin framework NAFS-1. In a recent study reported by Coronado et al., a multilayer thin film of NAFS-1 was deposited on 1-dodecylphosphonic acid (C12P) soaked permalloy (Py) substrate, Py-C12P. The resistance (*R*) of the MOF thin film at different thicknesses (*d*) was measured with a Hg drop top electrode and AFM.¹¹² A shallow dependence between *R* and *d* suggested that hopping was the primary mechanism responsible for the charge transport, and, as a consequence, for the conduction properties of this framework.^{112, 113}

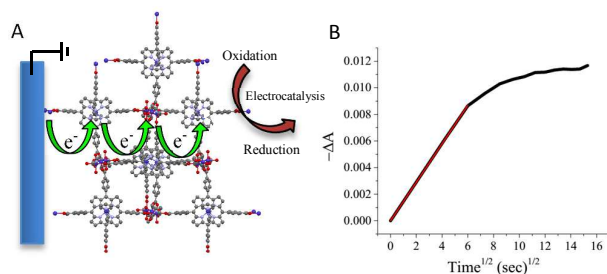


Figure 5. (A) A scheme of solvothermally grown CoPIZA thin film on FTO substrate. (B) Determination of apparent diffusion coefficient from the change of absorption at 419 nm of the ($\text{Co}^{\text{II/I}}\text{TCPP}$) redox couple in CoPIZA.¹¹¹

5. Redox Hopping in MOF Electrocatalysts

The examples discussed above clearly demonstrate the relevance of redox hopping to charge transport in electroactive frameworks. Currently, the interplay between electronic conductivity (determined by direct resistivity measurements) and redox hopping rate (derived from time-dependent electrochemical experiments), is still not fully understood.⁴⁶ A few reported electrocatalytic MOFs, where redox hopping was identified as a key mechanism for supplying the charge to the catalytic process,^{21, 23, 25, 29, 35, 39, 114} were found to be poor electrical conductors.^{24, 37} Nevertheless, several reports demonstrated that this process was capable of supplying charge to catalytic centers and of driving electrocatalytic transformations with high efficiency.^{24, 37, 39} Several factors, including the activity and the spatial arrangement of the catalyst, electroactive site coverage, and the thin film properties play important roles in dictating the performance of MOF electrocatalysts.

Incorporation of efficient catalysts and the variation of the linkers used in the construction of the framework were demonstrated to be feasible strategies to modify the electrocatalytic performance. Yaghi et al. built a Co porphyrin based covalent organic framework (COF)

as a CO_2 reduction electrocatalyst (COFs are a family of porous materials related to MOFs, but with structure supported by covalent bonds). An electronic absorption spectroelectrochemical study revealed a Cottrell type diffusion controlled redox hopping behavior in these materials. A potential step (-0.57 V vs RHE) was applied to COF-366-Co thin film while recording the absorption at 640 nm as a function of time. A relatively moderate D_{app} value of $2 \times 10^{-12} \text{ cm}^2/\text{s}$ was calculated by fitting the resultant data. The framework exhibited a remarkable turnover number up to 290000 with Faradaic efficiency reaching as high as 90%.³⁷ To test the effect of pore size on catalysis, Yaghi et al. expanded two isostructural frameworks, COF-366-Co and COF-367-Co. The cobalt porphyrin centers were connected by 1,4-benzenedicarboxaldehyde (BDA) in COF-366-Co and biphenyl-4,4'-dicarboxaldehyde (BPDA) in COF-367-Co. Based on BET surface area analysis, the pore size distribution of the frameworks increased from 10-18 Å in COF-366-Co to 12-23 Å in COF-367-Co. Larger pore size resulted in a higher CO_2 adsorption and therefore more rapid diffusion of both reactants/products and counter-ions. Thus, COF-367-Co exhibited higher catalytic current and lower overpotential for CO_2 reduction, compared to COF-366-Co under the same conditions. In addition, the percentage of electroactive cobalt centers increased from 4% in COF-366-Co to 8% in COF-367-Co, providing further support for diffusion controlled redox behavior.

Increasing the percentage of accessible electroactive sites could lead to the enhancement of a catalytic response under the same catalysts' loading level. It should be noted that less than 10% of the cobalt catalysts in the frameworks described above are electrochemically addressable. The authors attributed this low site availability to poor electrical contact between the electrode and deposited COF particles. Direct film growth during the framework synthesis is a promising option to alleviate this issue. Hupp et al. developed an alternative approach broadly applicable to a wide variety of MOF powders. In the report, colloidal NU-1000 particles carrying a negative charge were attached to the FTO electrode by electrophoretic deposition (EPD). Increasing deposition time resulted in an increase in the percentage of electrochemically accessible TBzPy linkers. Prolonged EPD time produced highly dense films comprised of MOF particle aggregates. Due to effective particle-to-particle redox hopping, more than 95% of the linkers were active in the NU-1000 thin film fabricated over the course of 180 min.¹¹⁵ This study demonstrated that electrochemical site accessibility could be increased through optimization of thin film fabrication techniques. Furthermore, it highlighted that the redox hopping properties within the particle can be modelled with high accuracy due to the regular, highly ordered nature of most MOF structures with well-defined positioning and orientation of redox centers.

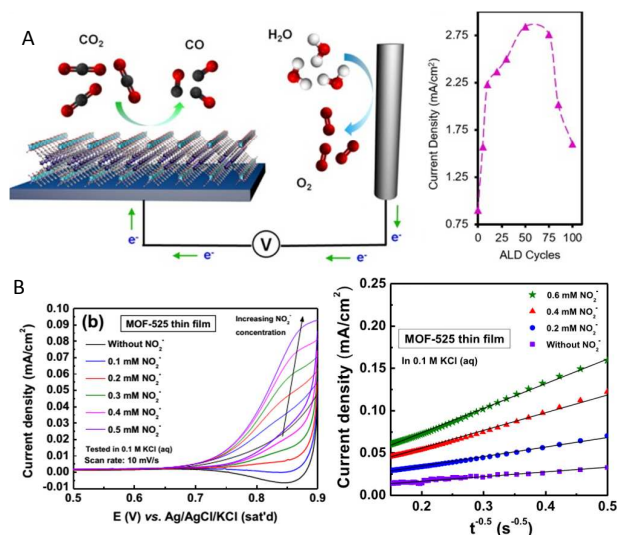


Figure 6. (A) Depiction of $\text{Al}_2(\text{OH})_2\text{TCPP-Co}$ film as an electrochemical CO_2 reduction catalyst and the relationship between the catalytic current density and the number of ALD cycles;³⁵ (B) CVs of MOF-525 thin film measured in the presence of varying amounts of nitrite, showing the increase in catalytic current with increasing substrate concentration. Based on the J vs $t^{-0.5}$ plots, obtained from the potential step experiments (0.9 V), it was determined that the D_{app} also increased when more nitrite was present in the solution.¹¹⁴

Moreover, controlling thickness and morphology of the MOF thin film is particularly advantageous for facilitating rapid charge and mass transport throughout the structure. Yang and Yaghi et al. employed this design strategy to obtain an efficient CO_2 reduction catalyst containing Co-TCPP catalysts, which also serve as bridging linkers to form the electrocatalytic $[\text{Al}_2(\text{OH})_2\text{TCPP-Co}]$ framework.³⁵ To achieve this, a nanosized Al thin film was first formed on the substrate by atomic layer deposition (ALD). Next, a $[\text{Al}_2(\text{OH})_2\text{TCPP-Co}]$ MOF thin film was grown by heating the Al coated electrode at 140°C in the DMF/water mixture in the presence of Co-TCPP linker. Cathodic peak current at -0.4 and -0.5 V, as well as anodic peak current at -0.2 V vs RHE exhibited a linear relationship with respect to $v^{1/2}$. This result confirmed the diffusion limited redox nature of the redox processes in these nanosized MOF thin films. Varying the cycle number of ALD can be used for precise control of the film thickness with the values ranging from 10 nm to 30–70 nm, when the cycle number was increased from 5 to 50. The catalytic current density at -0.57 V vs RHE increased as the number

of ALD cycles increased from 0 to 50. Interestingly, further increases in the film thickness led to a drop in the catalytic current. (Figure 6A). The authors attributed this effect to the balance of charge hopping and reactant/product diffusion to and from the bulk electrolyte. A similar conclusion was drawn by Marinescu et al. who investigated electrochemical H_2 reduction using a CoBHT (BHT = benzenehexathiolate) framework as a catalyst. The maximum catalytic current was attained for 244 nm thick films with further increases in thickness (1000 nm) causing a drop in the performance.¹¹⁶

6. Is Redox Hopping Sufficient to Drive MOF-based Electrocatalysis?

As discussed earlier, for a MOF with redox hopping as its primary mode of electron transport, careful optimization of the framework thin film parameters could produce highly efficient electrocatalytic materials. In this section, we aim to qualitatively evaluate the effect of the redox hopping rate upon MOF electrocatalytic performance, and also attempt to answer the core question: is a conductive framework necessary, or is charge transport via redox hopping enough to drive efficient electrocatalysis?

The focus of the discussion is the relationship between the steady state catalytic current, I_{cat} , and the parameter diagnostic of the redox hopping rate in the MOF thin films, D_{app} . For the majority of electroactive MOFs, the measurement of D_{app} was made by analyzing the current response after a potential step below the onset of catalytic current. The resultant potential bias will oxidize or reduce all the electrochemically accessible redox centers. Therefore, the corresponding current is the result of a semi-infinite diffusion process. However, at potentials sufficient to drive catalysis, the electroactive species are continuously switching between redox states as they participate in the catalytic cycle. Presumably redox hopping will only occur in the layers close to the electrode surface.¹¹⁴ It was found that D_{app} of a porphyrin based MOF-525 thin film measured at catalytic potentials increased as the concentration of reactant increased (Figure 6B).¹¹⁴ Therefore, the value of D_{app} obtained under catalytic conditions does not simply represent the intrinsic charge hopping properties of the material. Consequently, the resultant catalytic current I_{cat} cannot be directly fitted to a semi-infinite diffusion model, and additional considerations are required to relate D_{app} with I_{cat} .

Herein, we propose a simple model to discuss the relationship between D_{app} and I_{cat} . For molecular catalysts operating under the simplest possible EC mechanism under certain potential bias, the one turnover cycle can be separated into two steps. The first step is pre-catalysis oxidation or reduction of the catalytic center to reach its active oxidation state, similar to a charging process. The second step involves the sequence of transformations required to convert a substrate to a product. These include the interaction of substrate with the active site, intramolecular electron transfer, and the release of the product. The time required to complete these two steps can be denoted as t_{q} and t_{cat} (s), respectively. Similar results can be expected in MOFs, since catalytic sites are typically immobilized inside a porous scaffold, and are equally accessible for the substrate molecules. The average time required for the active species to

complete the two steps in one catalytic cycle can be assigned as $t_{\text{MOF-q}}$ and $t_{\text{MOF-cat}}$. This assumes the second step remains unchanged between the species in solution and those confined inside the framework, $t_{\text{MOF-cat}} = t_{\text{cat}}$ for all active sites. $t_{\text{MOF-q}}$ and t_{q} , on the other hand, might differ due to the different nature of charge transport and diffusion. Thus, the overall turnover frequency for the same catalyst under homogeneous condition (TOF, s^{-1}) and inside the MOF (TOF', s^{-1}) is also expected to differ.

$$\text{TOF} = 1/(t_{\text{q}} + t_{\text{cat}}) \quad (6)$$

$$\text{TOF}' = 1/(t_{\text{MOF-q}} + t_{\text{MOF-cat}}) \quad (7)$$

It is reasonable to assume that TOF' will be lower than TOF if $t_{\text{MOF-q}}$ is larger than t_{q} (Equation 5), which means that the catalysis will be limited by charge transport.

Now, we can consider a relationship between I_{cat} and D_{app} via the intermediate parameter $t_{\text{MOF-q}}$. Assuming an electrode area of 1 cm^2 , given the charge passed per unit time during electrolysis, Q ($\text{C s}^{-1} \text{ cm}^2$), then the active site coverage, Γ (mol/cm^2) and the concentration of active sites in MOF thin films C (mol/cm^3) should be,

$$\Gamma = Q/nF\text{TOF}' \quad (8)$$

$$C = \Gamma/d \quad (9)$$

where n is the number of electron transferred in the reaction, F is Faraday constant, and d is the thickness of the MOF thin films that are involved with the catalytic turn over process. Assuming that redox hopping only occurs during the charging step $t_{\text{MOF-q}}$ as a semi-infinite diffusion process, and the charge passed in each turnover cycle, Q' (C/cm^2) is,

$$Q' = Q/\text{TOF}' \quad (10)$$

we can evaluate the D_{app} (cm^2/s) of the charge transport. Based on Anson equation,

$$D_{\text{app}} = Q'^2\pi/4n^2F^2A^2C^2t_{\text{MOF-q}} \quad (11)$$

From equations (7)–(11), we obtain an expression for D_{app} under all the assumptions mentioned above:

$$D_{\text{app}} = \pi d^2/4t_{\text{MOF-q}} = \pi d^2/4(1/\text{TOF}' - t_{\text{MOF-cat}}) \quad (12)$$

For equation (12), it is important to note that:

- (1) $t_{\text{MOF-cat}}$ should be always smaller than $1/\text{TOF}'$.
- (2) The range of the possible values of d is implicitly related to Γ . For most molecular catalysts, the surface coverage of a fully packed monolayer, γ , is usually between 10^{-9} to $10^{-11} \text{ mol/cm}^2$. For a given Γ and the thickness of a catalyst monolayer, l (nm), the minimum value of film thickness should therefore be:

$$d_{\text{min}} = \Gamma/\gamma l \text{ (nm)} \quad (13)$$

If TOF' and $t_{\text{MOF-cat}}$ are constant, then the minimum redox hopping rate $D_{\text{app-min}}$ would be measured at d_{min} .

- (3) The benchmark current, I_{cat} , required for a commercially feasible catalytic MOF thin film should reach at least 10 mA/cm^2 .^{40,41} Thus, the Q discussed here will be 0.01 C/cm^2 .
- (4) For simplicity, the possible dependence of the magnitude of D_{app} with respect to the concentration of active sites was omitted from the calculations (although it is noted that previous experimental work supports such behavior for MOF films).²³

Considering a CO_2 to CO reduction reaction ($n = 2$), when $I_{\text{cat}} = 10 \text{ mA/cm}^2$, $\gamma = 10^{-10} \text{ mol/cm}^2$, $l = 1 \text{ nm}$, $d_{\text{min}} \geq l$ and $t_{\text{MOF-cat}}$ is constant, as TOF' increases, $D_{\text{app-min}}$ decrease accordingly (Figure 7). A relatively low $D_{\text{app-min}}$ value (10^{-12} - $10^{-10} \text{ cm}^2/\text{s}$) is adequate to support 10 mA/cm^2 catalytic current density when the TOF' of the incorporated catalyst is high and the thickness of the MOF film is small. For example, to support a 10 mA/cm^2 steady state catalytic current, if $t_{\text{MOF-cat}}$ is 0.01 s and the overall TOF' is 10 s^{-1} , the calculated d_{min} should be $\sim 52 \text{ nm}$ and the corresponding $D_{\text{app-min}}$ is readily attainable $2.3 \times 10^{-10} \text{ cm}^2/\text{s}$.^{23,117} It is possible to realize this scenario since there are already several electrochemical CO_2 reduction catalysts¹¹⁸ with TOF' higher than 100 s^{-1} reported and there are techniques available for fabrication of MOF thin films on the nanometer scale.

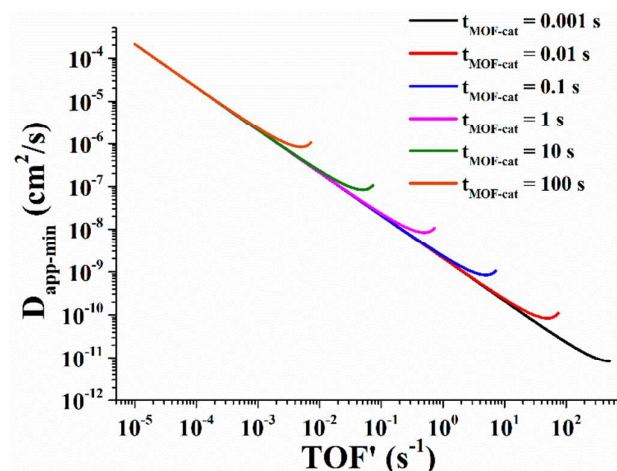


Figure 7. For electrochemical CO_2 reduction (CO_2 to CO) facilitated by a MOF thin film (assuming $I_{\text{cat}} = 10 \text{ mA/cm}^2$, $\gamma = 10^{-10} \text{ mol/cm}^2$, $l = 1 \text{ nm}$ and $d_{\text{min}} \geq l$), the expected $D_{\text{app-min}}$ with respect to the TOF' calculated at different $t_{\text{MOF-cat}}$ and d_{min} .

In practice, activation of the catalyst, namely transferring n electrons per site, usually involves one or multiple redox processes occurring at different potentials. Currently, the reported D_{app} values are mostly obtained from a single redox process and do not consider the entire activation process. Careful experimental design for accurate determination of $D_{\text{app-min}}$ is necessary to make more meaningful comparisons between different catalytic systems. Considering that the $D_{\text{app-min}}$ values obtained from our simple model are in the same range as D_{app} reported in literature, it seems evident that redox hopping is indeed sufficient to support electrocatalysis in MOFs. More precise evaluation of the redox transport rate in MOF thin films would require the in-depth analysis and measurement of the

intrinsic diffusion properties under catalytic conditions. For instance, the coefficients for electronic (D_e) and ionic (D_i) diffusions could be elucidated from theoretical modeling¹¹⁹⁻¹²¹ and experimental measurements.^{82, 122-124}

7. Conclusion

The rate of electrocatalysis in MOF thin films is controlled by not only the charge transport properties of the material but also the kinetics of the incorporated catalyst, as well as the diffusion of reactants/products and counter-ions. In this report, we evaluated the possibility of MOF-based electrocatalysis supported entirely by a redox hopping process. From our simple catalytic model, this mode of charge transport is indeed capable of supplying the necessary charge across the framework. These results provide practical guidelines for designing and improving existing MOF electrocatalysts. These include: (1) incorporating catalytic centers with high TOF; (2) increasing the coverage of uniformly distributed active sites in the framework; (3) optimizing the shape and dimensions of pore channels to enable rapid mass transport; and (4) decreasing the thickness and improving the quality of MOF film fabricated on the electrode.^{125, 126} Several other considerations related to MOF electrocatalysis are worth mentioning here. First, catalytic activity of molecular catalysts might be altered when incorporated inside MOF due to the structural modification and the altered chemical environment of the compound. In addition, the ideal reaction conditions for homogeneous catalysis might not be suitable for its corresponding MOF electrocatalyst. Some MOFs in particular are not stable in basic/acid aqueous solution and specific buffer solutions (e.g. phosphate buffer), as well as over particular potential ranges. Careful consideration is required to optimize the electrocatalysis reaction condition for MOF materials. Finally, evidence has shown that material transformation/degradation can occur to MOF electrocatalysts during a reaction. Therefore, it is necessary to conduct elaborate characterization (PXRD, SEM, ICP-MS, surface area analysis etc.) of MOF and MOF thin film electrocatalyst before and after the reaction, to confirm the integrity of MOF electrocatalysts. Further research to address these challenges is important for realizing the future applications of efficient and stable MOF electrocatalysts.

Acknowledgement

This material is based upon work supported by the National Science Foundation under Grant No. 1551964.

Conflicts of interest

There are no conflicts to declare.

References

1. I. Stassen, N. Burtch, A. Talin, P. Falcaro, M. Allendorf and R. Ameloot, *Chemical Society Reviews*, 2017, **46**, 3185-3241.
2. K. J. Erickson, F. Léonard, V. Stavila, M. E. Foster, C. D. Spataru, R. E. Jones, B. M. Foley, P. E. Hopkins, M. D. Allendorf and A. A. Talin, *Advanced Materials*, 2015, **27**, 3453-3459.
3. X. Chen, Z. Wang, P. Lin, K. Zhang, H. Baumgart, E. Redel and C. Wöll, *ECS Transactions*, 2016, **75**, 119-126.
4. L. Sun, B. Liao, D. Sheberla, D. Kraemer, J. Zhou, E. A. Stach, D. Zakharov, V. Stavila, A. A. Talin and Y. Ge, *Joule*, 2017, **1**, 168-177.
5. M. E. Foster, J. D. Azoulay, B. M. Wong and M. D. Allendorf, *Chemical Science*, 2014, **5**, 2081-2090.
6. D. Y. Lee, D. V. Shinde, S. J. Yoon, K. N. Cho, W. Lee, N. K. Shrestha and S.-H. Han, *The Journal of Physical Chemistry C*, 2013, **118**, 16328-16334.
7. R. Kaur, K.-H. Kim, A. Paul and A. Deep, *Journal of Materials Chemistry A*, 2016, **4**, 3991-4002.
8. W. A. Maza, A. J. Haring, S. R. Ahrenholtz, C. C. Epley, S. Lin and A. J. Morris, *Chemical Science*, 2016, **7**, 719-727.
9. M. Alvaro, E. Carbonell, B. Ferrer, F. X. Llabrés i Xamena and H. Garcia, *Chemistry-A European Journal*, 2007, **13**, 5106-5112.
10. C. G. Silva, A. Corma and H. García, *Journal of Materials Chemistry*, 2010, **20**, 3141-3156.
11. M. Usman, S. Mendiratta and K. L. Lu, *Advanced Materials*, 2017, **29**.
12. P. C. Banerjee, D. E. Lobo, R. Middag, W. K. Ng, M. E. Shaibani and M. Majumder, *ACS applied materials & interfaces*, 2015, **7**, 3655-3664.
13. W. H. Li, K. Ding, H. R. Tian, M. S. Yao, B. Nath, W. H. Deng, Y. Wang and G. Xu, *Advanced Functional Materials*, 2017.
14. L. Wang, Y. Han, X. Feng, J. Zhou, P. Qi and B. Wang, *Coordination Chemistry Reviews*, 2016, **307**, 361-381.
15. D. Feng, T. Lei, M. R. Lukatskaya, J. Park, Z. Huang, M. Lee, L. Shaw, S. Chen, A. A. Yakovenko and A. Kulkarni, *Nature Energy*, 2018, **1**.
16. M. B. Solomon, T. L. Church and D. M. D'Alessandro, *CrystEngComm*, 2017.
17. M. C. So, G. P. Wiederrecht, J. E. Mondloch, J. T. Hupp and O. K. Farha, *Chemical Communications*, 2015, **51**, 3501-3510.
18. T. Zhang and W. Lin, *Chemical Society Reviews*, 2014, **43**, 5982-5993.
19. M. Nasalevich, M. Van der Veen, F. Kapteijn and J. Gascon, *CrystEngComm*, 2014, **16**, 4919-4926.
20. C. A. Downes and S. C. Marinescu, *ChemSusChem*, 2017, **10**, 4374-4392.
21. B. A. Johnson, A. Bhunia and S. Ott, *Dalton Transactions*, 2017, **46**, 1382-1388.
22. C.-W. Kung, J. E. Mondloch, T. C. Wang, W. Bury, W. Hoffeditz, B. M. Klahr, R. C. Klet, M. J. Pellin, O. K. Farha and J. T. Hupp, *ACS applied materials & interfaces*, 2015, **7**, 28223-28230.
23. S. Lin, Y. Pineda - Galvan, W. A. Maza, C. C. Epley, J. Zhu, M. C. Kessinger, Y. Pushkar and A. J. Morris, *ChemSusChem*, 2017, **10**, 514-522.
24. X.-F. Lu, P.-Q. Liao, J.-W. Wang, J.-X. Wu, X.-W. Chen, C.-T. He, J.-P. Zhang, G.-R. Li and X.-M. Chen, *J. Am. Chem. Soc.*, 2016, **138**, 8336-8339.
25. P. M. Usov, S. R. Ahrenholtz, W. A. Maza, B. Stratakes, C. C. Epley, M. C. Kessinger, J. Zhu and A. J. Morris, *Journal of Materials Chemistry A*, 2016, **4**, 16818-16823.

COMMUNICATION

Journal Name

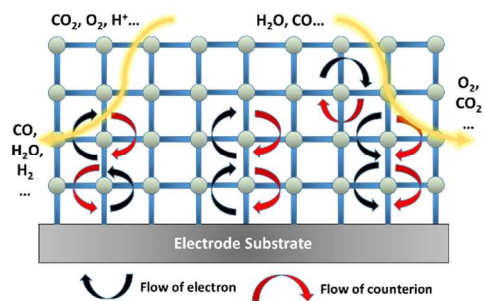
26. J.-Q. Shen, P.-Q. Liao, D.-D. Zhou, C.-T. He, J.-X. Wu, W.-X. Zhang, J.-P. Zhang and X.-M. Chen, *Journal of the American Chemical Society*, 2017, **139**, 1778-1781.
27. P. Manna, J. Debgupta, S. Bose and S. K. Das, *Angewandte Chemie International Edition*, 2016, **55**, 2425-2430.
28. Y. Gong, H.-F. Shi, Z. Hao, J.-L. Sun and J.-H. Lin, *Dalton Transactions*, 2013, **42**, 12252-12259.
29. P. M. Usov, B. Huffman, C. C. Epley, M. C. Kessinger, J. Zhu, W. A. Maza and A. J. Morris, *ACS Applied Materials & Interfaces*, 2017.
30. J. Mao, L. Yang, P. Yu, X. Wei and L. Mao, *Electrochemistry Communications*, 2012, **19**, 29-31.
31. M. Lions, J.-B. Tommasino, R. Chattot, B. Abeykoon, N. Guillou, T. Devic, A. Demessence, L. Cardenas, F. Maillard and A. Fateeva, *Chemical Communications*, 2017, **53**, 6496-6499.
32. R. Dong, M. Pfeffermann, H. Liang, Z. Zheng, X. Zhu, J. Zhang and X. Feng, *Angewandte Chemie International Edition*, 2015, **54**, 12058-12063.
33. A. J. Clough, J. W. Yoo, M. H. Mecklenburg and S. C. Marinescu, *Journal of the American Chemical Society*, 2014, **137**, 118-121.
34. R. Dong, Z. Zheng, D. C. Tranca, J. Zhang, N. Chandrasekhar, S. Liu, X. Zhuang, G. Seifert and X. Feng, *Chemistry-A European Journal*, 2017, **23**, 2255-2260.
35. N. Kornienko, Y. Zhao, C. S. Kley, C. Zhu, D. Kim, S. Lin, C. J. Chang, O. M. Yaghi and P. Yang, *J. Am. Chem. Soc.*, 2015, **137**, 14129-14135.
36. C.-W. Kung, C. O. Audu, A. W. Peters, H. Noh, O. K. Farha and J. T. Hupp, *ACS Energy Letters*, 2017, **2**, 2394-2401.
37. S. Lin, C. S. Diercks, Y.-B. Zhang, N. Kornienko, E. M. Nichols, Y. Zhao, A. R. Paris, D. Kim, P. Yang and O. M. Yaghi, *Science*, 2015, **349**, 1208-1213.
38. L. Ye, J. Liu, Y. Gao, C. Gong, M. Addicoat, T. Heine, C. Wöll and L. Sun, *Journal of Materials Chemistry A*, 2016, **4**, 15320-15326.
39. I. Hod, M. D. Sampson, P. Deria, C. P. Kubiak, O. K. Farha and J. T. Hupp, *ACS Catalysis*, 2015, **5**, 6302-6309.
40. Y. Gorlin and T. F. Jaramillo, *Journal of the American Chemical Society*, 2010, **132**, 13612-13614.
41. C. Liu, N. P. Dasgupta and P. Yang, *Chemistry of Materials*, 2013, **26**, 415-422.
42. T. Neumann, J. Liu, T. Wächter, P. Friederich, F. Symalla, A. Welle, V. Mugnaini, V. Meded, M. Zharnikov and C. Wöll, *ACS nano*, 2016, **10**, 7085-7093.
43. S. Patwardhan and G. C. Schatz, 2015.
44. S. Han, S. C. Warren, S. M. Yoon, C. D. Malliakas, X. Hou, Y. Wei, M. G. Kanatzidis and B. A. Grzybowski, *Journal of the American Chemical Society*, 2015, **137**, 8169-8175.
45. C. F. Leong, P. M. Usov and D. M. D'Alessandro, *MRS Bulletin*, 2016, **41**, 858-864.
46. L. Sun, M. G. Campbell and M. Dincă, *Angewandte Chemie International Edition*, 2016, **55**, 3566-3579.
47. P. M. Usov, C. F. Leong and D. M. D'Alessandro, in *Functional Supramolecular Materials*, 2017, pp. 247-280.
48. S. Takaishi, M. Hosoda, T. Kajiwara, H. Miyasaka, M. Yamashita, Y. Nakanishi, Y. Kitagawa, K. Yamaguchi, A. Kobayashi and H. Kitagawa, *Inorganic chemistry*, 2008, **48**, 9048-9050.
49. H. Miyasaka, *Accounts of chemical research*, 2012, **46**, 248-257.
50. P. Huo, T. Chen, J.-L. Hou, L. Yu, Q.-Y. Zhu and J. Dai, *Inorganic chemistry*, 2016, **55**, 6496-6503.
51. C. Leong, B. Chan, T. Faust and D. D'Alessandro, *Chemical Science*, 2014, **5**, 4724-4728.
52. L. E. Darago, M. L. Aubrey, C. J. Yu, M. I. Gonzalez and J. R. Long, *J. Am. Chem. Soc.*, 2015, **137**, 15703-15711.
53. R. Murase, C. F. Leong and D. M. D'Alessandro, *Inorganic Chemistry*, 2017, **56**, 14373-14382.
54. L. Sun, C. H. Hendon, S. S. Park, Y. Tulchinsky, R. Wan, F. Wang, A. Walsh and M. Dincă, *Chemical Science*, 2017, **8**, 4450-4457.
55. A. A. Talin, A. Centrone, A. C. Ford, M. E. Foster, V. Stavila, P. Haney, R. A. Kinney, V. Szalai, F. El Gabaly and H. P. Yoon, *Science*, 2013, 1246738.
56. X. Huang, P. Sheng, Z. Tu, F. Zhang, J. Wang, H. Geng, Y. Zou, C.-a. Di, Y. Yi and Y. Sun, *Nature communications*, 2015, **6**.
57. M. D. Allendorf, M. E. Foster, F. Léonard, V. Stavila, P. L. Feng, F. P. Doty, K. Leong, E. Y. Ma, S. R. Johnston and A. A. Talin, *The journal of physical chemistry letters*, 2015, **6**, 1182-1195.
58. A. Sengupta, S. Datta, C. Su, T. S. Heng, J. Ding, J. J. Vittal and K. P. Loh, *ACS applied materials & interfaces*, 2016, **8**, 16154-16159.
59. I. Hod, O. K. Farha and J. T. Hupp, *Chemical Communications*, 2016, **52**, 1705-1708.
60. C.-W. Kung, T.-H. Chang, L.-Y. Chou, J. T. Hupp, O. K. Farha and K.-C. Ho, *Chemical Communications*, 2015, **51**, 2414-2417.
61. Y. Kobayashi, B. Jacobs, M. D. Allendorf and J. R. Long, *Chemistry of Materials*, 2010, **22**, 4120-4122.
62. C. Avendano, Z. Zhang, A. Ota, H. Zhao and K. R. Dunbar, *Angewandte Chemie International Edition*, 2011, **50**, 6543-6547.
63. L. Sun, T. Miyakai, S. Seki and M. Dincă, *Journal of the American Chemical Society*, 2013, **135**, 8185-8188.
64. Z. Zhang, H. Zhao, H. Kojima, T. Mori and K. R. Dunbar, *Chemistry-A European Journal*, 2013, **19**, 3348-3357.
65. L. Sun, C. H. Hendon, M. A. Minier, A. Walsh and M. Dincă, *J. Am. Chem. Soc.*, 2015, **137**, 6164-6167.
66. J. Ferraris, D. Cowan, V. t. Walatka and J. Perlstein, *Journal of the American Chemical Society*, 1973, **95**, 948-949.
67. Y.-R. Qin, Q.-Y. Zhu, L.-B. Huo, Z. Shi, G.-Q. Bian and J. Dai, *Inorganic chemistry*, 2010, **49**, 7372-7381.
68. T. C. Narayan, T. Miyakai, S. Seki and M. Dincă, *Journal of the American Chemical Society*, 2012, **134**, 12932-12935.
69. S. S. Park, E. R. Hontz, L. Sun, C. H. Hendon, A. Walsh, T. Van Voorhis and M. Dincă, *J. Am. Chem. Soc.*, 2015, **137**, 1774-1777.
70. D. Sheberla, L. Sun, M. A. Blood-Forsythe, S. I. Er, C. R. Wade, C. K. Brozek, A. n. Aspuru-Guzik and M. Dincă, *Journal of the American Chemical Society*, 2014, **136**, 8859-8862.
71. M. G. Campbell, D. Sheberla, S. F. Liu, T. M. Swager and M. Dincă, *Angewandte Chemie International Edition*, 2015, **54**, 4349-4352.
72. A. J. Clough, J. M. Skelton, C. A. Downes, A. A. De La Rosa, J. W. Yoo, A. Walsh, B. C. Melot and S. C. Marinescu, *Journal of the American Chemical Society*, 2017, **139**, 10863-10867.

73. J.-H. Dou, L. Sun, Y. Ge, W. Li, C. H. Hendon, J. Li, S. Gul, J. Yano, E. A. Stach and M. Dincă, *Journal of the American Chemical Society*, 2017, **139**, 13608-13611.
74. T. Kambe, R. Sakamoto, K. Hoshiko, K. Takada, M. Miyachi, J.-H. Ryu, S. Sasaki, J. Kim, K. Nakazato and M. Takata, *Journal of the American Chemical Society*, 2013, **135**, 2462-2465.
75. J. Cui and Z. Xu, *Chemical Communications*, 2014, **50**, 3986-3988.
76. D. D'Alessandro, *Chemical Communications*, 2016, **52**, 8957-8971.
77. R. W. Murray, *Accounts of Chemical Research*, 1980, **13**, 135-141.
78. M. Kaneko, *Progress in polymer science*, 2001, **26**, 1101-1137.
79. H. S. White, J. Leddy and A. J. Bard, *Journal of the American Chemical Society*, 1982, **104**, 4811-4817.
80. F. B. Kaufman, A. H. Schroeder, E. M. Engler and V. V. Patel, *Applied Physics Letters*, 1980, **36**, 422-425.
81. K. Shigehara, N. Oyama and F. C. Anson, *Journal of the American Chemical Society*, 1981, **103**, 2552-2558.
82. N. A. SurrIDGE, C. S. Sosnoff, R. Schmehl, J. S. Facci and R. W. Murray, *The Journal of Physical Chemistry*, 1994, **98**, 917-923.
83. D. A. Buttry and F. C. Anson, *Journal of Electroanalytical Chemistry and Interfacial Electrochemistry*, 1981, **130**, 333-338.
84. A. H. Schroeder, F. B. Kaufman, V. Patel and E. M. Engler, *Journal of Electroanalytical Chemistry and Interfacial Electrochemistry*, 1980, **113**, 193-208.
85. M. Yagi, T. Mitsumoto and M. Kaneko, *Journal of Electroanalytical Chemistry*, 1997, **437**, 219-223.
86. F. Kaufman, A. Schroeder, E. Engler, S. Kramer and J. Chambers, *Journal of the American Chemical Society*, 1980, **102**, 483-488.
87. P. Daum and R. W. Murray, *Journal of Electroanalytical Chemistry and Interfacial Electrochemistry*, 1979, **103**, 289-294.
88. F. B. Kaufman and E. M. Engler, *Journal of the American Chemical Society*, 1979, **101**, 547-549.
89. H. Dahms, *The Journal of Physical Chemistry*, 1968, **72**, 362-364.
90. I. Ruff and V. Friedrich, *The Journal of Physical Chemistry*, 1971, **75**, 3297-3302.
91. I. Ruff, V. Friedrich, K. Demeter and K. Csillag, *The Journal of Physical Chemistry*, 1971, **75**, 3303-3309.
92. J. Saveant, *Journal of electroanalytical chemistry and interfacial electrochemistry*, 1986, **201**, 211-213.
93. F. C. Anson, D. N. Blauch, J. M. Saveant and C. F. Shu, *Journal of the American Chemical Society*, 1991, **113**, 1922-1932.
94. M. Yagi and T. Sato, *The Journal of Physical Chemistry B*, 2003, **107**, 4975-4981.
95. J. Facci, R. Schmehl and R. W. Murray, *Journal of the American Chemical Society*, 1982, **104**, 4959-4960.
96. J. M. Saveant, *The Journal of Physical Chemistry*, 1988, **92**, 1011-1013.
97. J. M. Saveant, *The Journal of Physical Chemistry*, 1988, **92**, 4526-4532.
98. C. P. Andrieux and J. Saveant, *The Journal of Physical Chemistry*, 1988, **92**, 6761-6767.
99. D. N. Blauch and J. M. Saveant, *Journal of the American Chemical Society*, 1992, **114**, 3323-3332.
100. C. R. Martin, I. Rubinstein and A. J. Bard, *Journal of the American Chemical Society*, 1982, **104**, 4817-4824.
101. M. Buda, G. Kalyuzhny and A. J. Bard, *Journal of the American Chemical Society*, 2002, **124**, 6090-6098.
102. F. P. Zamborini, M. C. Leopold, J. F. Hicks, P. J. Kulesza, M. A. Malik and R. W. Murray, *Journal of the American Chemical Society*, 2002, **124**, 8958-8964.
103. P. Daum, J. Lenhard, D. Rolison and R. W. Murray, *Journal of the American Chemical Society*, 1980, **102**, 4649-4653.
104. D. M. Oglesby, S. H. Omang and C. N. Reilley, *Analytical Chemistry*, 1965, **37**, 1312-1316.
105. K. Hirai, H. Uehara, S. Kitagawa and S. Furukawa, *Dalton transactions*, 2012, **41**, 3924-3927.
106. I. Hod, W. Bury, D. M. Gardner, P. Deria, V. Roznyatovskiy, M. R. Wasielewski, O. K. Farha and J. T. Hupp, *The journal of physical chemistry letters*, 2015, **6**, 586-591.
107. C. R. Wade, M. Li and M. Dincă, *Angewandte Chemie*, 2013, **125**, 13619-13623.
108. J. E. Halls, A. Hernán-Gómez, A. D. Burrows and F. Marken, *Dalton Transactions*, 2012, **41**, 1475-1480.
109. P. M. Usov, C. Fabian and D. M. D'Alessandro, *Chemical Communications*, 2012, **48**, 3945-3947.
110. S. Lin, A. K. Ravari, J. Zhu, P. M. Usov, M. Cai, S. R. Ahrenholtz, Y. Pushkar and A. J. Morris, *ChemSusChem*, 2018.
111. S. R. Ahrenholtz, C. C. Epley and A. J. Morris, *Journal of the American Chemical Society*, 2014, **136**, 2464-2472.
112. V. Rubio-Giménez, S. Tatay, F. Volatron, F. J. Martínez-Casado, C. Martí-Gastaldo and E. Coronado, *Journal of the American Chemical Society*, 2016, **138**, 2576-2584.
113. J. Liu, T. Wächter, A. Imler, P. G. Weidler, H. Gliemann, F. Pauly, V. Mugnaini, M. Zharnikov and C. Wöll, *ACS applied materials & interfaces*, 2015, **7**, 9824-9830.
114. C.-W. Kung, T.-H. Chang, L.-Y. Chou, J. T. Hupp, O. K. Farha and K.-C. Ho, *Electrochemistry Communications*, 2015, **58**, 51-56.
115. I. Hod, W. Bury, D. M. Karlin, P. Deria, C. W. Kung, M. J. Katz, M. So, B. Klahr, D. Jin and Y. W. Chung, *Advanced Materials*, 2014, **26**, 6295-6300.
116. C. A. Downes, A. J. Clough, K. Chen, J. W. Yoo and S. C. Marinescu, *ACS applied materials & interfaces*, 2017.
117. B. Johnson, A. Bhunia, H. Fei, S. Cohen and S. Ott, *Journal of the American Chemical Society*, 2018.
118. C. Costentin, M. Robert and J.-M. Savéant, *Chemical Society Reviews*, 2013, **42**, 2423-2436.
119. U. Schroöder, K. B. Oldham, J. C. Myland, P. J. Mahon and F. Scholz, *Journal of Solid State Electrochemistry*, 2000, **4**, 314-324.
120. M. Lovrić and F. Scholz, *Journal of Solid State Electrochemistry*, 1999, **3**, 172-175.
121. M. Lovrić and F. Scholz, *Journal of Solid State Electrochemistry*, 1997, **1**, 108-113.
122. A. Doménech, H. García, M. T. Doménech-Carbó and F. Llabrés-i-Xamena, *The Journal of Physical Chemistry C*, 2007, **111**, 13701-13711.
123. P. Pickup and R. W. Murray, *Journal of the American Chemical Society*, 1983, **105**, 4510-4514.
124. C. A. C. Paula J. Celis-Salazar, Spencer R. Ahrenholtz, Meng Cai, Charity C. Epley, Pavel M. Usov, Amanda J. Morris, *In preparation*, 2018.

COMMUNICATION

Journal Name

125. J. Liu and C. Wöll, *Chemical Society Reviews*, 2017, **46**, 5730-5770.
126. M. C. So, S. Jin, H.-J. Son, G. P. Wiederrecht, O. K. Farha and J. T. Hupp, *Journal of the American Chemical Society*, 2013, **135**, 15698-15701.



A perspective on redox hopping charge transport through metal organic frameworks and its role in driving efficient electrocatalysis.